M. Maestrini, P. Di Lizia, F. Topputo
Analytical Impulsive-To-continuous Thrust Conversion in Linearized Relative Dynamics
Journal of Guidance Control and Dynamics, In press - Published online 31/01/2021
doi:10.2514/1.G005520

Analytical Impulsive-to-Continuous Thrust Conversion in Linearized Relative Dynamics

Michele Maestrini*
Polytechnic University of Milan, 20156 Milan, Italy

Pierluigi Di Lizia†
Polytechnic University of Milan, 20156 Milan, Italy

Francesco Topputo‡
Polytechnic University of Milan, 20156 Milan, Italy

I. Introduction

Over the past few decades, space debris has become a persistent and a growing issue for space operations around the Earth. As emphasized in [1], an average of four to five break-ups per year occur in orbit, increasing debris and the probability of collisions. Consequently, active debris removal missions are of recent interest. Unmanned on-orbit servicing missions are currently being investigated for their commercial attractiveness: expensive satellites in constellations may benefit from the presence of autonomous on-orbit inspectors capable of monitoring the presence of external damages or solar panel degradation. The collected information could be exploited to plan a servicing mission. For the envisioned scenarios, a chaser has to operate autonomously in the vicinity of a non-cooperative target, whose characteristics might not be well known. This in turn involves the need of spacecraft guidance planning algorithms that can be efficiently executed on board, and that can meet stringent safety and observation constraints, which render classical direct and indirect trajectory optimization approaches hard to solve without proper tuning of the algorithms and appropriate selection of initial guesses.

Guidance approaches have historically exploited linear dynamics [2] and natural motion trajectories obtained via impulsive maneuvers [3–5] to plan relative navigation trajectories. Linear models have also been exploited in recent studies of Motion Planning algorithms [6, 7]. These algorithms were developed in the field of autonomous driving and they represent an active research domain in the robotics industry. Their attractiveness is owed to their low computational burden, which is useful on limited-resource systems. Since proximity operations require small orbital separations, and due to the need of computing and ranking a large number of trajectories efficiently, linear dynamics and impulsive ΔV maneuvers are often the preferred assumptions in motion planning algorithms [8–14]. Despite being used also in state-of-the-art experiments [15], impulsive maneuvers are a limiting assumption especially for low-thrust systems, which can lead to suboptimality. Therefore, there is the need to convert these impulsive maneuvers to finite burns.

*PhD Candidate, Department of Aerospace Science and Technology, michele.maestrini@polimi.it.
†Assistant Professor, Department of Aerospace Science and Technology, pierluigi.dilizia@polimi.it, AIAA Member.
‡Associate Professor, Department of Aerospace Science and Technology, francesco.topputo@polimi.it, AIAA Member.

In the past, many studies were dedicated to the solution of this problem, which were motivated by the desire of using readily available impulsive solutions as a basis for an optimization with finite thrust control to aid convergence. Initial approaches [16, 17] used constants of motion to estimate an initial guess of the problem's costate variables, which were fed to an iterative procedure to retrieve acceptable acceleration values. Works [18, 19] employed a series expansion in the inverse thrust acceleration and exhaust velocity in terms of the costates of the optimal impulsive trajectory. The state of the art work presented in [20] builds upon [21], which is similar in purpose to past studies but differs in the conversion methodology from the impulsive solution. In fact, despite being introduced for multiple maneuver conversion and optimization, the key step of the method in [21] is the conversion of a single impulsive maneuver to a linearly steered burn with constant thrust. This conversion requires an optimization process to guarantee time and state continuity at the maneuver point. An iteration-free polynomial alternative to the linearly steered thrust vector is presented in this paper to convert a ΔV into a continuous thrust solution. The proposed control analytically guarantees final constraint satisfaction in the linearized dynamics. A solution for the envisioned problem can be retrieved in analytical closed-form for an energy optimal problem [22, 23]. However, the obtained control functions are complicated, and require a numerical iterative procedure to obtain the upper bound of the required thrust and to impose that its maximum value is not exceeded. On the contrary, the control law proposed in this work has a mathematical analytic bound used to reliably estimate the required transfer time to guarantee that the maximum thrust constraint is not violated.

Favored by its analytic and iteration-free nature, the transformation can be embedded into on-board guidance planning algorithms without affecting numerical efficiency and enabling an on-line assessment of the consequences of a bounded, continuous thrust. The resulting control law is compared against the solution of minimum-energy, minimum-time, and minimum-fuel optimal control problems in terms of propellant consumption and transfer time.

The paper is organized as follows. After deriving the analytic control law in Section II, the energy-optimal linear quadratic control and the setup for the fuel and time optimal problems are addressed in Sections III and IV, respectively. The assessment of the results on numerical test cases is presented in Section V. Section VI concludes the paper.

II. Analytical Impulsive to Continuous Thrust Conversion

This section is devoted to derive the analytical conversion from an impulsive $\mathbf{\Delta V}$ to a continuous thrust maneuver. The conversion is derived in the dynamical framework governed by the linear Clohessy-Wiltshire (CW) equations [2], which assume a circular target trajectory about a central body with standard gravitational parameter μ:

$$\begin{aligned} \ddot{x} &= 3x + 2\dot{y} \\ \ddot{y} &= -2\dot{x} \\ \ddot{z} &= -z \end{aligned} \tag{1}$$

where x, y, and z are components of the chaser position relative to the target along unit vectors **i**, **j**, and **k** respectively, as illustrated in Figure 1. In Eqs. (1), distances are scaled to the target orbital radius R_t, which provides the length unit LU = R_t, whereas time is scaled with the inverse of the mean orbital motion of the target $n = \sqrt{\mu/R_t^3}$, which provides the time unit TU = $1/n$. The reference frame used is often referred to as Local-Vertical-Local-Horizontal (LVLH). The **i** unit vector represents the Local-Vertical, and it is directed along the orbital position of the target spacecraft, whereas the **k** unit vector is normal to the orbital plane and parallel to the orbital angular momentum of the target. The **j** vector represents the Local-Horizontal direction and completes the right-handed triad.

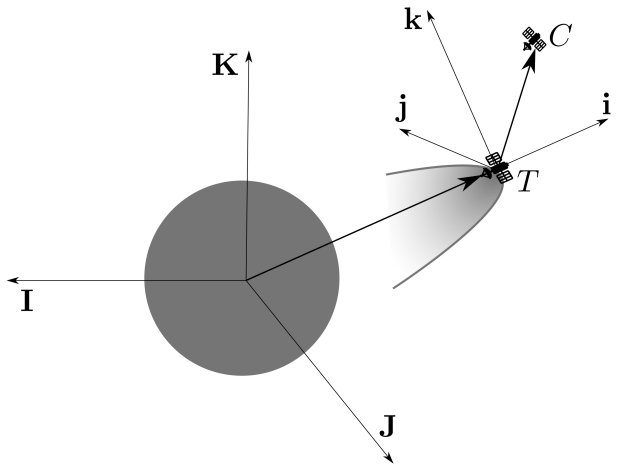

Fig. 1 Reference frame of the CW equations (T and C refer to the target and the chaser, respectively).

Given the velocity change vector $\mathbf{\Delta V}$ with magnitude ΔV applied to an initial state $\mathbf{x}_0 = [x_0, y_0, z_0, \dot{x}_0, \dot{y}_0, \dot{z}_0]^\top$ at time t_0, Eq. (1) can be solved in closed-form for the resulting trajectory. More specifically, assuming the components of $\mathbf{\Delta V} = [\delta u, \delta v, \delta w]^\top$ expressed in the LVLH reference frame, the solution at any time t can be found by adding this impulsive maneuver to the initial velocity [2]:

$$
\begin{aligned}
x(t) &= -(3x_0 + 2\dot{y}_0 + 2\delta v)\cos(t) + (\dot{x}_0 + \delta u)\sin(t) + 4x_0 + 2\dot{y}_0 + 2\delta v \\
y(t) &= (2\dot{x}_0 + 2\delta u)\cos(t) + (6x_0 + 4\dot{y}_0 + 4\delta v)\sin(t) - (6x_0 + 3\dot{y}_0 + 3\delta v)t + y_0 - 2\dot{x}_0 - 2\delta u \\
z(t) &= z_0\cos(t) + (\dot{z}_0 + \delta w)\sin(t) \\
\dot{x}(t) &= (3x_0 + 2\dot{y}_0 + 2\delta v)\sin(t) + (\dot{x}_0 + \delta u)\cos(t) \\
\dot{y}(t) &= (-2\dot{x}_0 - 2\delta u)\sin(t) + (6x_0 + 4\dot{y}_0 + 4\delta v)\cos(t) - 6x_0 - 3\dot{y}_0 - 3\delta v \\
\dot{z}(t) &= -z_0\sin(t) + (\dot{z}_0 + \delta w)\cos(t)
\end{aligned}
\tag{2}
$$

If a continuous thrust with acceleration components that implicitly depends on time $U(t)$, $V(t)$ and $W(t)$ is assumed

for the chaser, the CW equations become:

$$\begin{aligned} \ddot{x} &= 3x + 2\dot{y} + U(t) \\ \ddot{y} &= -2\dot{x} + V(t) \\ \ddot{z} &= -z + W(t) \end{aligned} \tag{3}$$

Two alternative impulsive-to-continuous thrust conversion approaches are derived, which will be referred to as "forward" and "backward" conversions, respectively. In the forward conversion, the continuous thrust starts at t_0 and the aim of the conversion is to build analytical closed-form solutions for $U(t)$, $V(t)$, and $W(t)$, such that the controlled trajectory generated by Eq. (3) reaches the same position and velocity of Eq. (2) at a final time $t = t_f$. Conversely, in the backward conversion, the continuous thrust starts earlier than the maneuver epoch on the original trajectory and the analytical closed-form solutions for $U(t)$, $V(t)$, and $W(t)$ are built to reach the desired final trajectory at maneuver time, matching both position and velocity with included impulsive maneuver. By properly combining the forward and backward conversions, the proposed approach can map two consecutive maneuvers separated by a coasting arc, which is a typical application example in proximity operations. In this scenario, the first impulsive maneuver is converted with the forward approach and the end state will be located on the transfer manifold between the initial and final impulsive maneuvers. On the other hand, the second impulsive maneuver is converted backward, i.e. the continuous thrust starts from the transfer manifold and ends at the location of the second impulsive maneuver, matching the final position and velocity with the final ΔV applied. A schematized representation of the forward and backward approaches is given in Figure 2.

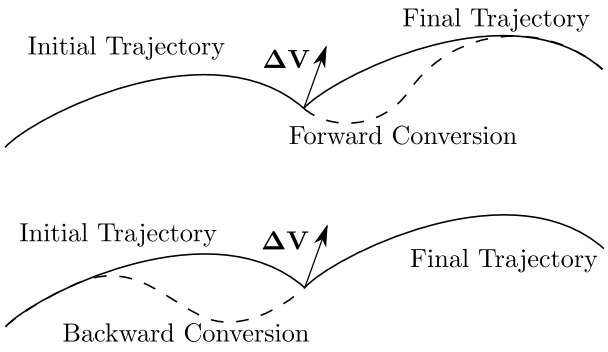

Fig. 2 Illustration of the forward conversion (top) and backward conversion (bottom).

The z component and the corresponding solution for $W(t)$ are addressed first, as they are decoupled from the other two equations. In their derivation, the forward conversion is presented first; then, the key passages to retrieve the backward solution are presented. The x and y components are then treated together to obtain $U(t)$ and $V(t)$ due to the coupled nature of the motion in the **ij** plane. For these components, the forward conversion is presented, whereas the backward conversion is only reported in terms of its results for the sake of conciseness.

A. Solution for $W(t)$

The general solution of Eq. (3) for z is given by a homogeneous term (i.e. $z_h(t)$) and a particular solution (i.e. $z_p(t)$) associated to $W(t)$:

$$\begin{aligned} z(t) &= z_h(t) + z_p(t) = a_z \cos(t) + b_z \sin(t) + z_p(t) \\ \dot{z}(t) &= \dot{z}_h(t) + \dot{z}_p(t) = -a_z \sin(t) + b_z \cos(t) + \dot{z}_p(t) \end{aligned} \tag{4}$$

where a_z and b_z represent the constant coefficients of the homogeneous solution of the second-order differential equation. The evaluation of Eq. (4) at $t_0 = 0$ and the use of the initial condition $\mathbf{x}_0$ provide the following relations:

$$\begin{aligned} z_0 &= a_z + z_{p,0} \\ \dot{z}_0 &= b_z + \dot{z}_{p,0} \end{aligned} \tag{5}$$

where $z_{p,0} = z_p(0)$ and $\dot{z}_{p,0} = \dot{z}_p(0)$. Solving Eq. (5) for a_z and b_z, and substituting in Eq. (4) yields

$$\begin{aligned} z(t) &= (z_0 - z_{p,0}) \cos(t) + (\dot{z}_0 - \dot{z}_{p,0}) \sin(t) + z_p(t) \\ \dot{z}(t) &= -(z_0 - z_{p,0}) \sin(t) + (\dot{z}_0 - \dot{z}_{p,0}) \cos(t) + \dot{z}_p(t) \end{aligned} \tag{6}$$

To map the impulsive maneuver with the forward conversion, it is necessary to express z and $\dot{z}$ with Eq. (2) at an arbitrary final time.

$$\begin{aligned} z(t_f) &= z_0 \cos(t_f) + (\dot{z}_0 + \delta w) \sin(t_f) \\ \dot{z}(t_f) &= -z_0 \sin(t_f) + (\dot{z}_0 + \delta w) \cos(t_f) \end{aligned} \tag{7}$$

Conversely, in the backward conversion, z and $\dot{z}$ at t_f must be obtained by setting the initial impulsive maneuver to zero as $\delta u = \delta v = \delta w = 0$ in Eq. (2). Then, the final impulsive maneuver will be applied at final time t_f. With this method, z and $\dot{z}$ at t_f become

$$\begin{aligned} z(t_f) &= z_0 \cos(t_f) + \dot{z}_0 \sin(t_f) \\ \dot{z}(t_f) &= -z_0 \sin(t_f) + \dot{z}_0 \cos(t_f) + \delta w \end{aligned} \tag{8}$$

To obtain the forward boundary conditions for $z_p(t)$, a system of conditions is created by equating the coefficients

of the sine, cosine, and constant terms at t_f in Eq. (7) and Eq.(6).

$$\begin{aligned} z_p(t_f) &= z_{p,f} = 0 \\ \dot{z}_p(t_f) &= \dot{z}_{p,f} = 0 \\ z_p(0) &= z_{p,0} = 0 \\ \dot{z}_p(0) &= \dot{z}_{p,0} = -\delta w \end{aligned} \tag{9}$$

Instead, to obtain the backward boundary conditions for $z_p(t)$, a system of conditions is created by equating the coefficients of the sine, cosine, and constant terms at t_f in Eq. (8) and Eq.(6).

$$\begin{aligned} z_p(t_f) &= z_{p,f} = 0 \\ \dot{z}_p(t_f) &= \dot{z}_{p,f} = \delta w \\ z_p(0) &= z_{p,0} = 0 \\ \dot{z}_p(0) &= \dot{z}_{p,0} = 0 \end{aligned} \tag{10}$$

The conditions in Eq. (9) and Eq. (10) can be satisfied by selecting $z_p(t)$ as a third order polynomial, which is the lowest degree polynomial necessary to impose all four boundary conditions. It appears evident that the proposed solution is here recast as a shape based trajectory design. The first instance of this method was the study of the logarithmic spiral as a low-thrust, absolute trajectory [24]. Several other shape functions followed, such as exponential sinusoid [25], high order inverse polynomials [26], and cosine inverse polynomials [27]. More recent methods investigated the use of finite Fourier series [28], Bezier functions [29], and linear exponential shapes to model pseudo-equinoctial elements [30]. The common drawback of these approaches is that some parameters need to be calculated by either by numerical solution of a system of nonlinear equations or via optimization methods. Optimization free (not iteration free) algorithms were developed in the state of the art work by Novak and Vasile [31] which uses ad hoc functions to shape spherical coordinates and was extended in [32] via the use of high order polynomials to model orbital elements. The approach proposed in this manuscript makes use of third order polynomials to shape the trajectory without iterative procedures. Based on this choice, the forward set of boundary conditions in Eq. (9) generates a particular shape for $z_p(t)$.

$$z_p(t) = -\frac{\delta w}{t_f^2} t^3 + 2\frac{\delta w}{t_f} t^2 - \delta w\, t \tag{11}$$

Substituting Eq. (11) into Eq. (6), we obtain the full homogeneous and particular solution for $z(t)$ and $\dot{z}(t)$. By further substitution of these expressions into Eq. (3), the forward input ${}^F W(t)$ is retrieved, where the left superscript F indicates

that the equation refers to the forward conversion.

$$ {}^{F}W(t) = -\frac{\delta w}{t_f^2}t^3 + 2\frac{\delta w}{t_f}t^2 - \delta w\left(\frac{6}{t_f^2} + 1\right)t + 4\frac{\delta w}{t_f} \tag{12} $$

If the same steps are followed for the backward boundary conditions in Eq. (10), the following control law is obtained, where the left superscript B indicates that the current equation refers to the backward conversion.

$$ {}^{B}W(t) = \frac{\delta w}{t_f^2}t^3 - \frac{\delta w}{t_f}t^2 + \delta w\frac{6}{t_f^2}t - 2\frac{\delta w}{t_f} \tag{13} $$

B. Solution for $U(t)$ and $V(t)$

In order to find a closed-form solution for $U(t)$ and $V(t)$, Eq. (3) is manipulated to derive two decoupled equations for x and y. The following procedure is valid for the forward conversion approach, and can be slightly modified to accommodate also the derivation of the backward conversion. The second order differential equations describing $\ddot{x}$ and $\ddot{y}$ are differentiated once and twice respectively, and the result is rearranged to obtain:

$$ \begin{aligned} \dddot{x} + \dot{x} &= f(t) \\ \dddot{y} + \ddot{y} &= g(t) \end{aligned} \tag{14} $$

where $f(t) = 2V(t) + \dot{U}(t)$ and $g(t) = \ddot{V}(t) - 3V(t) - 2\dot{U}(t)$. The general solution to Eq. (14) requires a homogeneous solution (i.e. $x_h(t)$ and $y_h(t)$) and a particular solution (i.e. $x_p(t)$ and $y_p(t)$):

$$ \begin{aligned} x(t) &= x_h(t) + x_p(t) = a_x\cos(t) + b_x\sin(t) + c_x + x_p(t) \\ y(t) &= y_h(t) + y_p(t) = a_y\cos(t) + b_y\sin(t) + c_y t + d_y + y_p(t) \end{aligned} \tag{15} $$

the coefficients a_x, b_x, c_x, a_y, b_y, c_y, and d_y in Eq. (15) are the constant coefficients for the homogeneous solution to the third-order and fourth-order differential equations shown in Eq. (14). They can be obtained by substituting $t = 0$ in

Eqs. (15) and in their derivatives:

$$\begin{aligned}
x_0 &= a_x + c_x + x_{p,0} \\
y_0 &= a_y + d_y + y_{p,0} \\
\dot{x}_0 &= b_x + \dot{x}_{p,0} \\
\dot{y}_0 &= b_y + c_y + \dot{y}_{p,0} \\
\ddot{x}_0 &= -a_x + \ddot{x}_{p,0} \\
\ddot{y}_0 &= -a_y + \ddot{y}_{p,0} \\
\dddot{y}_0 &= -b_y + \dddot{y}_{p,0}
\end{aligned} \tag{16}$$

where the subscript 0 is applied to a quantity to identify its value at $t_0 = 0$. Eq. (16) must be coupled with the following relations that can be inferred from Eq. (3) and the third order derivative of $y(t)$ taken during the decoupling process:

$$\begin{aligned}
\ddot{x}_0 &= 3x_0 + 2\dot{y}_0 + U_0 \\
\ddot{y}_0 &= -2\dot{x}_0 + V_0 \\
\dddot{y}_0 &= -6x_0 - 4\dot{y}_0 - 2U_0 + \dot{V}_0
\end{aligned} \tag{17}$$

where $U_0 = U(0)$, $V_0 = V(0)$, and $\dot{V}_0 = \dot{V}(0)$. The coefficients obtained from the solution of the system of equations provided by Eq. (16) and (17) are substituted into Eq. (15) to retrieve

$$\begin{aligned}
x(t) = \quad & (-3x_0 - 2\dot{y}_0 - U_0 + \ddot{x}_{p,0})\cos(t) + (\dot{x}_0 - \dot{x}_{p,0})\sin(t) + x_0 - x_{p,0} - \ddot{x}_{p,0} + 3x_0 + 2\dot{y}_0 + U_0 + x_p(t) \\
y(t) = \quad & (2\dot{x}_0 - V_0 + \ddot{y}_{p,0})\cos(t) + (6x_0 + 4\dot{y}_0 + 2U_0 - \dot{V}_0 + \dddot{y}_{p,0})\sin(t) + \\
& + t(\dot{V}_0 - \dot{y}_{p,0} - 6x_0 - 3\dot{y}_0 - 2U_0 - \ddot{y}_{p,0}) + y_0 - y_{p,0} - 2\dot{x}_0 + V_0 - \ddot{y}_{p,0} + y_p(t)
\end{aligned} \tag{18}$$

Similarly to the procedure followed for $W(t)$, a system of equations corresponding to Eq. (7) is set up also for x and y. The position resulting from Eq. (18) and the velocity obtained by taking its derivative, must be the same as the ones obtained with Eq. (2) at an arbitrary final time t_f. Consequently, the following conditions for the particular solutions $x_p(t)$, $y_p(t)$ and for the control accelerations $U(t)$ and $V(t)$ must apply:

$$\begin{aligned}
x_{p,0} &= 0 \qquad & y_{p0} &= 0 \\
\dot{x}_{p,0} &= -\delta u \qquad & \dot{y}_{p,0} &= -\delta v \\
x_{p,f} &= 0 \qquad & y_{pf} &= 0 \\
\dot{x}_{p,f} &= 0 \qquad & \dot{y}_{pf} &= 0
\end{aligned} \tag{19}$$

$$
\begin{aligned}
U_0 &= 2\delta v + \ddot{x}_{p,0} \\
V_0 &= -2\delta u + \ddot{y}_{p,0} \\
\dot{V}_0 &= 2U_0 - 4\delta v + \dddot{y}_{p,0}
\end{aligned}
\tag{20}
$$

The conditions in Eq. (19) can be satisfied by selecting the third order polynomial shape for $x_p(t)$ and $y_p(t)$, as it was done in Eq. (11):

$$
\begin{aligned}
x_p(t) &= -\tfrac{\delta u}{t_f^2} t^3 + 2\tfrac{\delta u}{t_f} t^2 - \delta u\, t \\
y_p(t) &= -\tfrac{\delta v}{t_f^2} t^3 + 2\tfrac{\delta v}{t_f} t^2 - \delta v\, t
\end{aligned}
\tag{21}
$$

By substituting Eq. (21) into Eq. (14), f and g can be retrieved.

$$
f(t) = -3\frac{\delta u}{t_f^2} t^2 + 4\frac{\delta u}{t_f} t - \delta u - 6\frac{\delta u}{t_f^2}
\tag{22}
$$

$$
g(t) = -6\frac{\delta v}{t_f^2} t + 4\frac{\delta v}{t_f}
\tag{23}
$$

To finally obtain the control accelerations $U(t)$ and $V(t)$, the following set of differential equations must be solved, with the initial conditions provided by Eq. (20):

$$
\begin{aligned}
\dot{U}(t) &= f(t) - 2V(t) \\
\ddot{V}(t) + V(t) &= 2f(t) + g(t)
\end{aligned}
\tag{24}
$$

This system of differential equations is a consequence of the decoupling process used for Eq. (14) and it is solved analytically to obtain a particular solution for $U(t)$ and $V(t)$, where the left superscript F indicates that the equation refers to the forward conversion approach.

$$
{}^{F}U(t) = 3\frac{\delta u}{t_f^2} t^3 + t^2\left(6\frac{\delta v}{t_f^2} - 6\frac{\delta u}{t_f}\right) - t\left(6\frac{\delta u}{t_f^2} + 8\frac{\delta v}{t_f} - 3\delta u\right) + 4\frac{\delta u}{t_f} + 2\delta v
\tag{25}
$$

$$
{}^{F}V(t) = -6\frac{\delta u}{t_f^2} t^2 + t\left(8\frac{\delta u}{t_f} - 6\frac{\delta v}{t_f^2}\right) + 4\frac{\delta v}{t_f} - 2\delta u
\tag{26}
$$

The procedure can be duplicated for the backward solution by changing the boundary conditions in Eq. (19) in a similar fashion as it was done to retrieve ${}^{B}W(t)$ in Section II.A. The outcome of this procedure are the backward control laws ${}^{B}U(t)$ and ${}^{B}W(t)$, where the left superscript B indicates that the equation refers to the backward conversion approach.

$$ {}^{B}U(t) = -3\frac{\delta u}{t_f^2}t^3 + t^2\left(-6\frac{\delta v}{t_f^2} + 3\frac{\delta u}{t_f}\right) + t\left(6\frac{\delta u}{t_f^2} + 4\frac{\delta v}{t_f}\right) - 2\frac{\delta u}{t_f} \tag{27} $$

$$ {}^{B}V(t) = 6\frac{\delta u}{t_f^2}t^2 + t\left(-4\frac{\delta u}{t_f} + 6\frac{\delta v}{t_f^2}\right) - 2\frac{\delta v}{t_f} \tag{28} $$

The controls in Eqs. (25), (26), and (12), as well as their backward counterparts Eqs. (27), (28), and (13) show a singularity for $t_f = 0$. However, this is acceptable as it would imply that the transfer between initial conditions and final manifold is instantaneous, which is never the case unless $\mathbf{\Delta V} = \mathbf{0}$.

C. Control bounds

Following a conservative approach, analytic upper bounds for ${}^{F}U(t)$, ${}^{F}V(t)$ and ${}^{F}W(t)$ are derived in this section and used hereafter to obtain the conditions that guarantee that the analytic control profile given by Eqs. (25), (26), and (12) does not exceed the maximum available thrust. The following procedure can be replicated for the backward controls given in Eqs. (27), (28), and (13), however this is not reported, as the same final bound is obtained. Hence, to simplify the notation, the left superscript is removed in the remainder of this section, and only the forward components of the control thrust are used. The component $W(t)$ has two possible expressions for its maximum value depending on t_f.

$$ W(t) \leq W_{\max} = \begin{cases} 4\frac{\delta w}{t_f} & \text{for} \quad t_f \leq \sqrt{6(3+2\sqrt{3})} \\ \frac{2\delta w\,(t_f^3 + (t_f^2-18)^{1.5})}{27t_f^2} & \text{for} \quad t_f > \sqrt{6(3+2\sqrt{3})} \end{cases} \tag{29} $$

The value of the maximum is located at $t/t_f = 0$, and its amplitude decreases for increasing final times until $t_f = \sqrt{6(3+2\sqrt{3})}$; then, it starts to grow again with t_f and moves away from $t/t_f = 0$. This trend is induced by the specific selection of a third order polynomial to approximate the shape of the particular solution. The particular choice of shape function influences the shape of the controls. An in depth investigation on different functions may yield controls that allow to obtain less conservative bounds. In particular, higher order polynomials with favourable extremal properties may provide additional degrees of freedom to exploit to improve the current solution. However, it is not guaranteed that such solutions will still be analytically available as for the functions selected in this work. In fact, the selection of third order polynomials allowed us to achieve the desired outcome of obtaining analytical closed-form controls and their bounds, hence the above consideration constitutes an interesting basis for further studies.

The maximum $W(t)$ for any impulsive maneuver is reached if the impulse is entirely provided along z, i.e. $\delta w = \Delta V$. Hence, a conservative upper bound $\overline{W}(t)$,which is represented in Figure 3, can be obtained using $\delta_w = \Delta V$ in Eq. (12). Thanks to Eq. (29), we can formulate an upper bounding value for the $W(t)$ control as:

$$W(t) \leq \overline{W}(t) \leq \overline{W}_{max} = \begin{cases} 4\frac{\Delta V}{t_f} & \text{for} \quad t_f \leq \sqrt{6(3+2\sqrt{3})} \\ \frac{2\Delta V\,(t_f^3+(t_f^2-18)^{1.5})}{27t_f^2} & \text{for} \quad t_f > \sqrt{6(3+2\sqrt{3})} \end{cases} \tag{30}$$

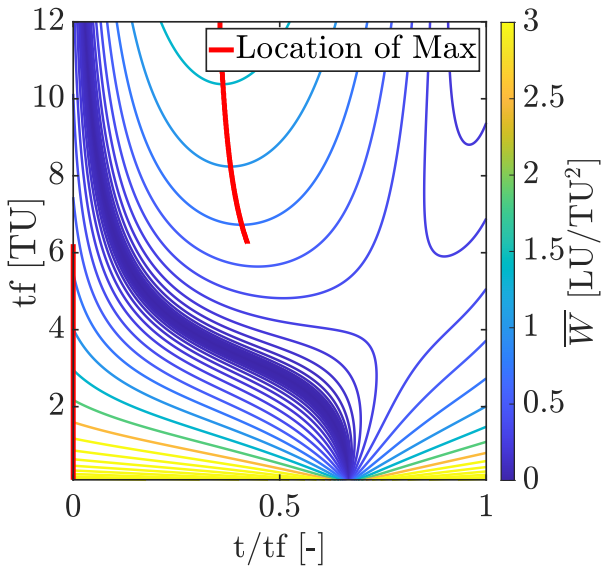

Fig. 3 Illustration of the amplitude of $\overline{W}(t)$ obtained for a unit ΔV as a function of final time t_f and maneuver completion ratio t/t_f.

Since $U(t)$ and $V(t)$ are linear in both δu and δv, their bounds can be obtained by treating them as planar surfaces, i.e. $U(t) = a_u(t)\delta u + b_u(t)\delta v$ (or $V(t) = a_v(t)\delta u + b_v(t)\delta v$) with time varying coefficients $a_u(t)$, $b_u(t)$, $a_v(t)$, and $b_v(t)$ obtained by collecting those terms which multiply δu and δv in Eqs. (25) and (26). The maximum value of these linear functions lies on the boundary of the region of admissible values of $(\delta u; \delta v)$. A conservative enclosure of this region is obtained by setting the whole ΔV in the **ij** plane as $\delta u^2 + \delta v^2 = \Delta V^2$, similarly to what was done for $W(t)$. Such approximation consists in selecting the direction of $\mathbf{\Delta V}$ which provides the maximum amplitude for the controls at any time t. This approach gives two conservative bounding functions $\overline{U}(t)$ for $U(t)$ and $\overline{V}(t)$ for $V(t)$, which are described by:

$$U(t) \leq \overline{U}(t) = \sqrt{a_u(t)^2 + b_u(t)^2}\Delta V \tag{31}$$

$$V(t) \leq \overline{V}(t) = \sqrt{a_v(t)^2 + b_v(t)^2}\Delta V \tag{32}$$

By maximizing Eq. (31) and Eq. (32) with respect to t, it is possible to obtain the maximum values in Eqs. (33) and

(34), which are once again located at $t/t_f = 0$.

$$U(t) \leq \overline{U}(t) \leq \overline{U}_{\max} = 2\Delta V \sqrt{1 + \frac{4}{t_f^2}} \quad \text{for} \quad t_f < t^U \tag{33}$$

$$V(t) \leq \overline{V}(t) \leq \overline{V}_{\max} = 2\Delta V \sqrt{1 + \frac{4}{t_f^2}} \quad \forall \quad t_f \tag{34}$$

In particular, the bound for $U(t)$ has been obtained by maximizing Eq. (31) with a symbolic solver, and the maximum reported in Eq. (33) is valid until $t^U \approx 3.7$ TU. Notice that this particular threshold of t_f is independent from the system parameters, and is determined by the choice of the third order polynomial for the particular solution of the problem. This allowed us to formulate the analytic bound for Eq. (31) only up until $t_f = t^U$, after this threshold, only a numerical solution for this bound could be retrieved. An illustration of the functions $\overline{V}(t)$ and $\overline{U}(t)$ is reported in Figure 4, where an arbitrary maximum final time is selected, as any $t_f \in (0, \infty)$ TU is admissible.

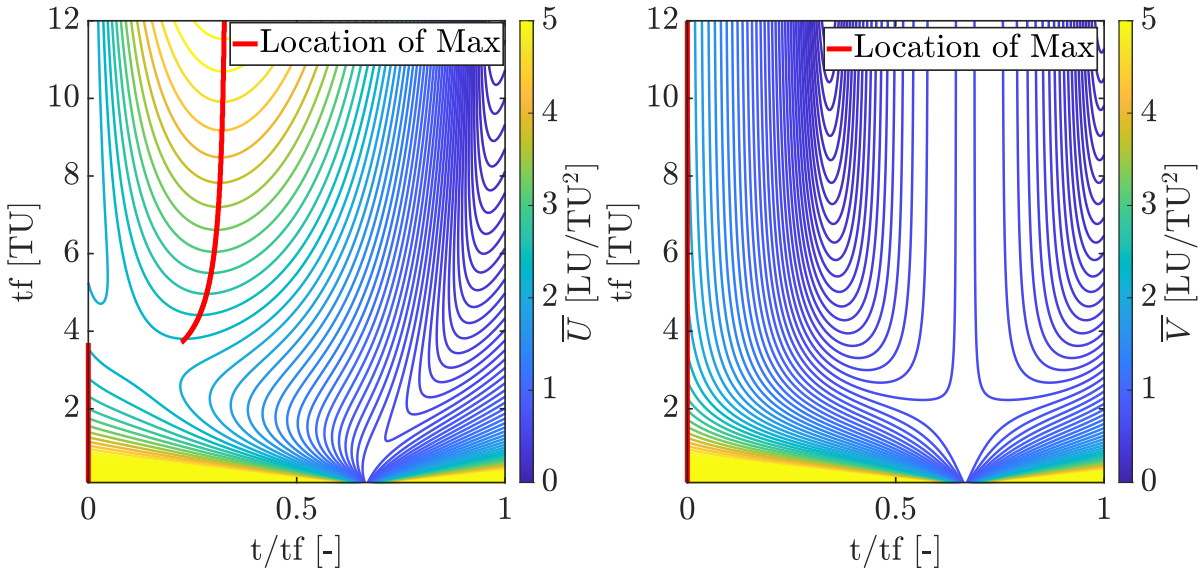

Fig. 4 Illustration of the amplitude of $\overline{U}(t)$ (left) and $\overline{V}(t)$ (right) obtained for a unit ΔV as a function of final time t_f and maneuver completion ratio t/t_f. The maximum location is always at $t/t_f = 0$ for $\overline{V}(t)$, whereas it is at $t/t_f = 0$ until $t_f = t^U$ for $\overline{U}(t)$. The selection of the maximum t_f used is arbitrary as any $t_f \in (0, \infty)$ TU is admissible.

By selecting the worst maneuver conditions for the three thrust directions, it is possible to obtain a conservative bound on the input acceleration $a_{\max}$ by summing up the worst case contributions given by Eq. (30), Eq. (33), and Eq. (34) as:

$$a_{\max} = \sqrt{U_{\max}^2 + V_{\max}^2 + W_{\max}^2} = \Delta V \sqrt{8 + \frac{48}{t_f^2}} \tag{35}$$

The maximum acceleration is obtained in $\mathrm{LU/TU}^2$, if we want to retrieve the equivalent thrust in Newton we can multiply it by the scaling constants used in this section. The maximum thrust deriving from the analytic control profile is:

$$T_{\max} = m_0\, n^2\, R_t\, \Delta V \sqrt{8 + \frac{48}{t_f^2}} \tag{36}$$

where m_0 is the spacecraft mass at the beginning of the thrusting phase, and provides the mass unit MU. Eq. (36) can be inverted to obtain an analytic expression for the minimum final time t_f required to convert the impulsive $\mathbf{\Delta V}$ into a continuously propelled trajectory that is guaranteed to never exceed the maximum available thrust T_{max}.

$$t_f = \sqrt{\frac{48}{\left(\frac{T_{max}}{m_0 n^2 R_t \Delta V}\right)^2 - 8}} \leq 3.7 \tag{37}$$

Overall, Eqs. (25), (26), and (12) analytically map any impulsive maneuver into a continuous control acceleration, whereas Eq. (37) provides the t_f that guarantees that the maximum available thrust is not exceeded (if the resulting $t_f \leq t^U$). It can be shown that the exact same control bound and requirement on t_f are retrieved for the backward controls of Eqs. (27), (28), and (13) if the procedure proposed in this section is applied. This fast analytic approach is particularly appealing for usage on limited resources systems.

III. Energy Optimal Linear-Quadratic Control

The direct counterpart of the proposed method is to solve the energy optimal control problem characterized by a quadratic cost function

$$J = \int_{t_0}^{t_f} \mathcal{L}\, \mathrm{d}t = \frac{1}{2} \int_{t_0}^{t_f} \mathbf{u}^\top \mathbf{u}\, \mathrm{d}t \tag{38}$$

where $\mathbf{u}(t) = [U(t), V(t), W(t)]^\top$, and subject to the linear dynamics given by Eq. (3), expressed conventionally as

$$\dot{\mathbf{x}} = \mathbf{A}\mathbf{x} + \mathbf{B}\mathbf{u} = \underbrace{\begin{bmatrix} 0 & 0 & 0 & 1 & 0 & 0 \\ 0 & 0 & 0 & 0 & 1 & 0 \\ 0 & 0 & 0 & 0 & 0 & 1 \\ 3 & 0 & 0 & 0 & 2 & 0 \\ 0 & 0 & 0 & -2 & 0 & 0 \\ 0 & 0 & -1 & 0 & 0 & 0 \end{bmatrix}}_{\mathbf{A}} \begin{pmatrix} x \\ y \\ z \\ \dot{x} \\ \dot{y} \\ \dot{z} \end{pmatrix} + \underbrace{\begin{bmatrix} 0 & 0 & 0 \\ 0 & 0 & 0 \\ 0 & 0 & 0 \\ 1 & 0 & 0 \\ 0 & 1 & 0 \\ 0 & 0 & 1 \end{bmatrix}}_{\mathbf{B}} \begin{pmatrix} U(t) \\ V(t) \\ W(t) \end{pmatrix} \tag{39}$$

where $\mathbf{x} = [x, y, z, \dot{x}, \dot{y}, \dot{z}]^\top$ is the state composed of positions and velocities. Introducing the co-state $\boldsymbol{\lambda}$, the Hamiltonian of the problem is given by

$$H = \mathcal{L} + \boldsymbol{\lambda}^\top(\mathbf{A}\mathbf{x} + \mathbf{B}\mathbf{u}) = \frac{1}{2}\mathbf{u}^\top\mathbf{u} + \boldsymbol{\lambda}^\top\mathbf{A}\mathbf{x} + \boldsymbol{\lambda}^\top\mathbf{B}\mathbf{u} \tag{40}$$

Consequently, the optimality conditions of this optimal control problem yield [22]:

$$\frac{\partial H}{\partial \mathbf{u}} = \mathbf{u} + \mathbf{B}^\top\boldsymbol{\lambda} = \mathbf{0} \tag{41}$$

$$\dot{\boldsymbol{\lambda}} = -\frac{\partial H}{\partial \mathbf{x}} = -\mathbf{A}^\top\boldsymbol{\lambda} \tag{42}$$

The optimal control problem is then solved by the following system of equations.

$$\mathbf{u} = -\mathbf{B}^\top\boldsymbol{\lambda} \tag{43}$$

$$\begin{pmatrix} \dot{\mathbf{x}} \\ \dot{\boldsymbol{\lambda}} \end{pmatrix} = \begin{bmatrix} \mathbf{A} & -\mathbf{B}\mathbf{B}^\top \\ \mathbf{0} & -\mathbf{A}^\top \end{bmatrix} \begin{pmatrix} \mathbf{x} \\ \boldsymbol{\lambda} \end{pmatrix} = \boldsymbol{\Omega} \begin{pmatrix} \mathbf{x} \\ \boldsymbol{\lambda} \end{pmatrix} \tag{44}$$

The matrix $\boldsymbol{\Omega}$ is constant, therefore we can find a closed-form solution to the system of ordinary differential equations.

$$\begin{pmatrix} \mathbf{x}(t) \\ \boldsymbol{\lambda}(t) \end{pmatrix} = e^{\boldsymbol{\Omega} t} \begin{pmatrix} \mathbf{x}_0 \\ \boldsymbol{\lambda}_0 \end{pmatrix} = \begin{bmatrix} e^{\boldsymbol{\Omega} t}_{xx} & e^{\boldsymbol{\Omega} t}_{x\lambda} \\ e^{\boldsymbol{\Omega} t}_{\lambda x} & e^{\boldsymbol{\Omega} t}_{\lambda\lambda} \end{bmatrix} \begin{pmatrix} \mathbf{x}_0 \\ \boldsymbol{\lambda}_0 \end{pmatrix} \tag{45}$$

Where $\mathbf{x}_0$ and $\boldsymbol{\lambda}_0$ are the initial state and co-state vectors. Given a desired final state $\mathbf{x}_f$ to be reached at an assigned final time t_f, the initial co-state vector can be obtained via inversion of Eq. (45).

$$\boldsymbol{\lambda}_0 = \left(e^{\boldsymbol{\Omega} t_f}_{x\lambda}\right)^{-1} \left(\mathbf{x}_f - e^{\boldsymbol{\Omega} t_f}_{xx}\,\mathbf{x}_0\right) \tag{46}$$

By combining Eq. (46) with Eq. (45), it is possible to obtain the optimal evolution of the state and co-state vectors:

$$\mathbf{x}(t) = e^{\boldsymbol{\Omega} t}_{xx}\,\mathbf{x}_0 + e^{\boldsymbol{\Omega} t}_{x\lambda}\left[\left(e^{\boldsymbol{\Omega} t_f}_{x\lambda}\right)^{-1}\left(\mathbf{x}_f - e^{\boldsymbol{\Omega} t_f}_{xx}\,\mathbf{x}_0\right)\right] \tag{47}$$

$$\boldsymbol{\lambda}(t) = e^{\boldsymbol{\Omega} t}_{\lambda x}\,\mathbf{x}_0 + e^{\boldsymbol{\Omega} t}_{\lambda\lambda}\left[\left(e^{\boldsymbol{\Omega} t_f}_{x\lambda}\right)^{-1}\left(\mathbf{x}_f - e^{\boldsymbol{\Omega} t_f}_{xx}\,\mathbf{x}_0\right)\right] \tag{48}$$

Eq. (48) can then be substituted in Eq. (43) to obtain the optimal control law in closed-form. Similarly to Section II, within the transfer problem addressed in this paper, $\mathbf{x}_f$ is obtained by evaluating Eq. (2) at the desired t_f. The control

action thus obtained is energy optimal, which provides an appealing solution for problems with unbounded control thrust. However, unlike the approach proposed in Section II, the resulting expressions cannot be easily manipulated to obtain an explicit analytic equation to compute t_f such that the constraint on the maximum thrust is not violated.

IV. Nonlinear Optimal Control Problem Statement

The analytic control law introduced in Section II is assessed against the results of a fuel-optimal (FO) and a time-optimal (TO) control problem. Both optimal control problems involve the Nonlinear Equations of Relative Motion (NERM) [33] around a target on a circular orbit of radius R_t about a body with standard gravitational parameter μ. In this setting, the mean motion is computed as $n = \sqrt{\mu/R_t}$. The control variables selected are two thrusting angles (i.e. θ and ϕ) and a throttle $u = T/T_{max}$.

$$\begin{aligned}
\ddot{x} &= 2n\dot{y} + n^2 x - \frac{\mu(R_t+x)}{[(R_t+x)^2+y^2+z^2]^{\frac{3}{2}}} + \frac{\mu}{R_t^2} + u\frac{T_{max}\cos\theta\cos\phi}{m} \\
\ddot{y} &= -2n\dot{x} + n^2 y - \frac{\mu y}{[(R_t+x)^2+y^2+z^2]^{\frac{3}{2}}} + u\frac{T_{max}\cos\theta\sin\phi}{m} \\
\ddot{z} &= -\frac{\mu z}{[(R_t+x)^2+y^2+z^2]^{\frac{3}{2}}} + u\frac{T_{max}\sin\theta}{m}
\end{aligned} \tag{49}$$

By defining the control acceleration vector as $\mathbf{a}_c = uT_{max}/m[\cos\theta\cos\phi\,,\ \cos\theta\sin\phi\,,\ \sin\theta]^\top$, it is possible to express the mass m variational equation as Eq. (50).

$$\dot{m} = -\frac{m||\mathbf{a}_c||}{c} = -u\frac{T_{max}}{c} \tag{50}$$

where $c = g_0 I_{sp}$ is the exhaust velocity, with g_0 the standard gravity and I_{sp} the specific impulse of the thruster. The control variables u (throttle), θ (inclination), and ϕ (azimuth) are illustrated in Figure 5, and they are subject to the following constraints:

$$\begin{aligned}
u &\in [0, 1] \\
\theta &\in [-\tfrac{\pi}{2}, \tfrac{\pi}{2}] \\
\phi &\in [0, 2\pi)
\end{aligned} \tag{51}$$

The optimization requires the final state to lie on the manifold $\boldsymbol{\psi}(t_f)$ describing the analytical solutions of the linear CW equations as described in Eq. (2). The objective function has the general form:

$$J = \int_0^{t_f} \mathcal{L}\,\mathrm{d}t \tag{52}$$

where $\mathcal{L} = 1$ for the TO problem and $\mathcal{L} = u$ for the FO problem. The optimization is solved with a direct transcription and collocation method as implemented in [34], where it is shown how an optimal control problem can be transformed

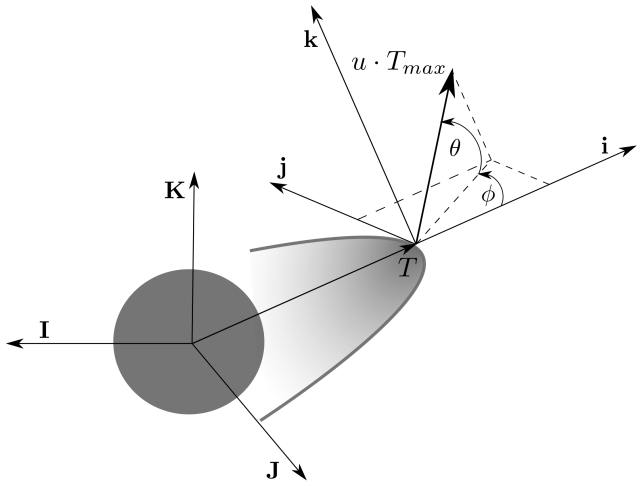

Fig. 5 Coordinates describing the control thrust direction in its LVLH components, in terms of amplitude and direction.

into an nonlinear programming (NLP) problem via direct transcription method. An NLP problem is a decisional problem concerning a scalar objective function, linear constraints and no dynamics involved, which can be solved with standard approaches [35].

All simulations are performed on a quad-core Intel processor i7-6700HQ, with an available RAM of 16GB and written in Matlab.

Table 1 Parameters of the problem taken from [13].

Physical Constant	Value
μ	$3.986 \cdot 10^{14}\ \frac{\mathrm{m}^3}{\mathrm{s}^2}$
$T_{\max}$	0.05 N
R_t	$7.0 \cdot 10^6$ m
I_{sp}	1000 s
g_0	$9.81\ \frac{\mathrm{m}}{\mathrm{s}^2}$
Length Unit (LU)	1000 m
Time Unit (TU)	$\sqrt{\frac{r^3}{\mu}} \approx 927.64$ s
Mass Unit (MU)	100 kg

V. Numerical Simulation

This section is focused on the assessment of the performance of the proposed analytic solution (AS) developed in Section II. The presented results are obtained via the forward analytic approach, as the backward counterpart will retrieve analogous results. The AS is compared to the energy optimal (EO) linear-quadratic control to provide its advantages and

disadvantages with respect to this control law. Additionally, AS is compared to the solution of the FO and TO control problems to quantify the suboptimality of the proposed approach in a nonlinear environment. To conclude, an example of the conversion of a two-impulse transfer is shown, which exploits both backward and forward conversion approaches.

A. Linear dynamics

First of all, the proposed analytic solution and the EO linear-quadratic control are compared in the linear dynamics of Eq. (1) using the parameters reported in Table 1 and taken from [13]. A set of 1000 random initial conditions of the chaser are sampled. Each component of the position is drawn from a uniform distribution with 0 m mean and 100 m interval amplitude. Whereas, each component of the velocity is drawn from a uniform distribution with 0 m/s mean and 0.11 m/s interval amplitude. The imparted $\mathbf{\Delta V}$ has random direction and the amplitude fixed to 0.09 m/s, in accordance to the maximum value allowed in [13]. The solutions of the Monte Carlo simulation are compared in terms of the integral of the throttle over the firing time $\int_0^{\bar{t}_f} u \, \mathrm{d}t$. Notice that in this particular definition of consumption $\bar{t}_f$ represents time expressed in seconds. Using the input optimal acceleration $\mathbf{u}$ from Eq. (43) and the mass computed with Eq. (50), the equivalent throttle for the EO problem can be computed as a thrust ratio $m||\mathbf{u}||/T_{max}$. To compute the equivalent throttle for the AS, we used the norm of the control acceleration with components ${}^F U(t)$, ${}^F V(t)$, and ${}^F W(t)$ from Eqs. (25), (26), and (12). The mean consumption obtained for the EO problem is 300.85 s with a standard deviation of 13.58 s, whereas the mean consumption of the AS yields 375.88 s with a standard deviation of 40.35 s. The time t_f to complete the maneuver is selected according to Eq. (37) with the parameters values in Table 1, which gives $t_f \approx 1.6082$ TU. The throttle (i.e. thrust ratio T/T_{max}) obtained by the EO and AS is illustrated in Figure 6. Notice that, for the particular choice of parameters, the EO solution satisfies the control bound, even though there is no mathematical guarantee as formulated for AS in subsection II.C. The maximum thrust of AS is never violated thanks to the choice of t_f according to Eq. (37), which meets the control bounds derived in subsection II.C.

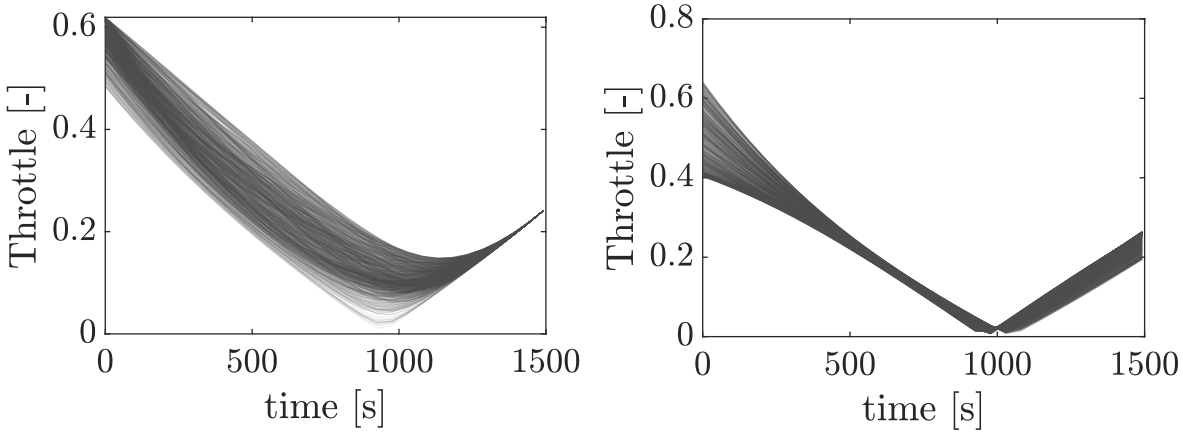

Fig. 6 Throttle obtained for the AS (left) and the EO (right) cases as resulting from 1000 random trials with different initial conditions and ΔV imparted.

B. Nonlinear dynamics

Having observed a limited performance degradation against the EO problem in the linear dynamics, the AS control is analyzed here when applied to the NERM dynamics. The accuracy is tested on the same samples of the Monte Carlo simulation carried out for the previous section. The forward analytic control law is applied to the NERM dynamics and propagated until the final time t_f computed with Eq. (37). The accuracy is assessed as the maximum norm of the state error at t_f between the NERM and the CW propagations. A sample solution trajectory is reported in Figure 7, where the error with respect to the target manifold obtained from Equation 2 by applying the same initial conditions and impulsive ΔV is reported for each component of the position and velocity vectors. The error in position and velocity is driven to approximately zero at the final time. The resulting control profile is illustrated in Figure 8. The results of the Monte Carlo simulation are summarized in Figure 9, where the mean error is ~ 7 mm for the position and ~ 0.02 mm/s for the velocity.

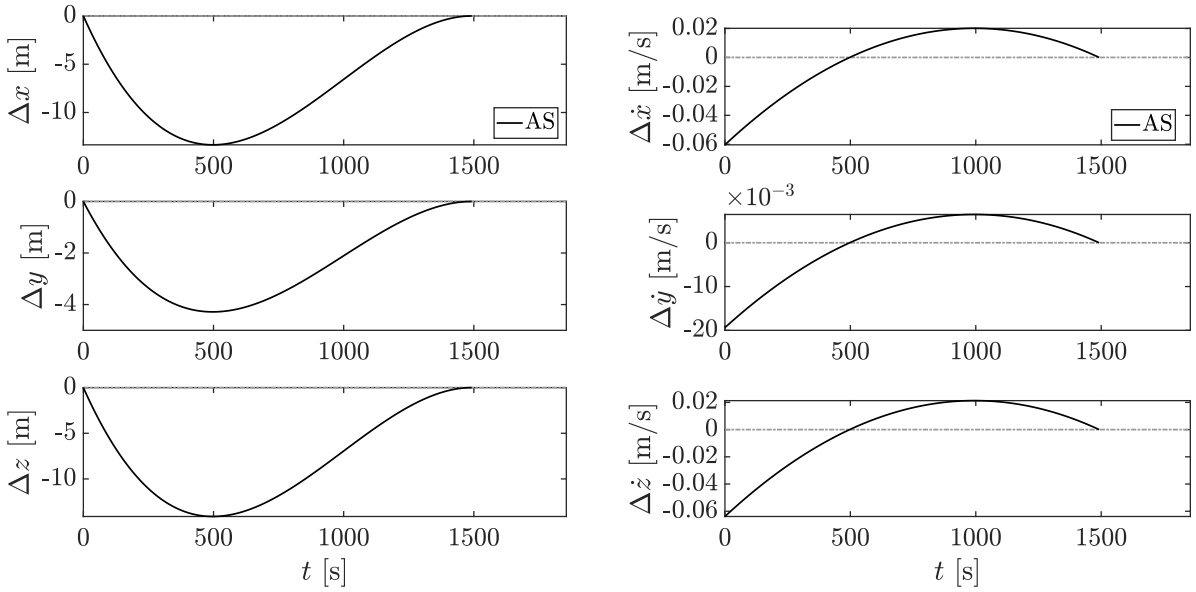

Fig. 7 Evolution of the position (left) and velocity (right) error obtained for a trial sample of initial conditions via the AS control conversion of a random ΔV.

The AS is then used as a feasible first guess for the numerical solution of the FO and TO problems in the NERM dynamics, and it guaranteed 100% convergence rate for both problems. The comparison between TO, FO, and AS is reported for one sample of the Monte Carlo analysis. The position and velocity errors with respect to the target trajectory are plotted in Figure 10, whereas Figure 11 shows the comparison in terms of control inputs. Even though AS is suboptimal, it is compared to the TO solution and to the FO solution to observe how they approach the same target manifold, starting from the same initial conditions. The solutions of the Monte Carlo simulation are also compared in Table 2 in terms of seconds required to complete the maneuver $\bar{t}_f$, and the integral of the throttle $\int_0^{\bar{t}_f} u \, \mathrm{d}t$. This

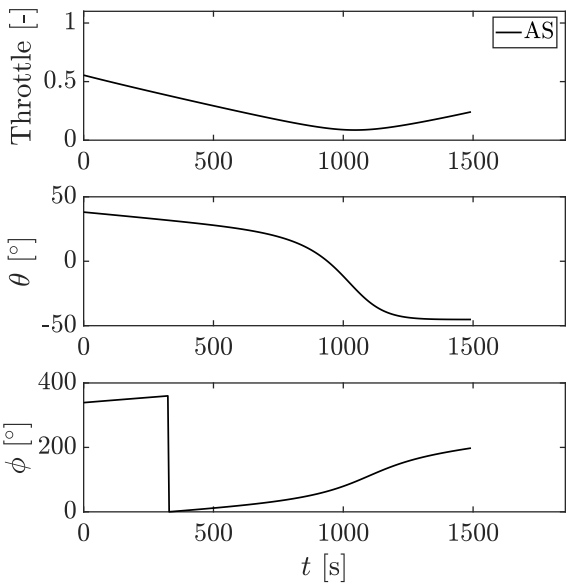

Fig. 8 Control history obtained for a sample trajectory applying AS.

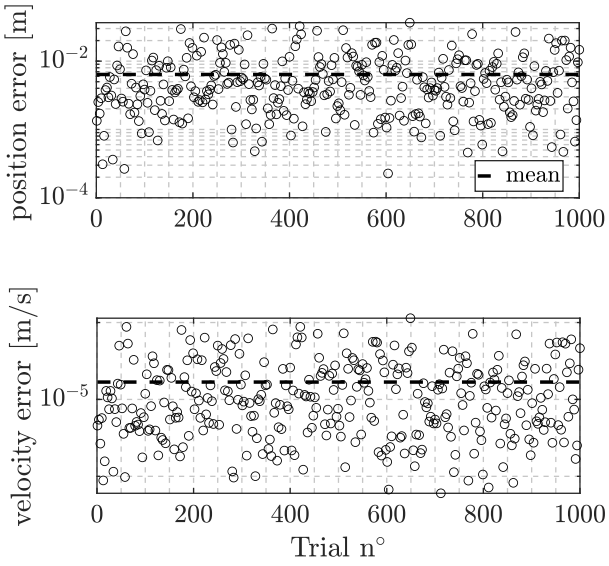

Fig. 9 Position and velocity error with respect to the target trajectory at t_f obtained by applying the analytic control law in the NERM dynamics.

analysis is meant to quantify the suboptimality of AS with respect to the TO and the FO problem. The time to complete the maneuver in the analytic case is selected according to Eq. (37) for the fixed ΔV amplitude of 0.09 m/s, therefore it shows no variation among the samples. Moreover, the throttle integral for the TO problem is equal to the time to complete the maneuver as the time optimal solution requires the throttle to be always on at 1.

The solver for the Monte Carlo simulation needed an average of approximately 50 iterations for the TO problem and

Table 2 Comparison of the solutions of the Monte Carlo simulation for the FO, TO, and AS cases in terms of dimensional consumption and resulting time to complete the maneuver.

Performance Parameter	**Time Optimal**	**Fuel Optimal**	**Analytic**
Throttle integral [s] *mean (standard deviation)*	439.63 (13.35)	130.89 (11.78)	375.88 (40.35)
Time [s] *mean (standard deviation)*	439.63 (13.35)	3332.55 (1258.90)	1491.83 (0.00)

400 iterations to solve the FO problem, with $N = 200$ discretization time instants. Even exploiting the sparsity and symmetry properties of the Jacobian and Hessian matrices involved in the solution of the optimization problem with the nonlinear programming approach, their size keeps growing quadratically with N, whereas the effort for computing the analytic control is given by the evaluation of three handle functions. On average, the FO problem required a 30 seconds run-time for convergence, whereas the TO problem required an average of 10 seconds. On the contrary the solution of the AS was obtained in the order of milliseconds.

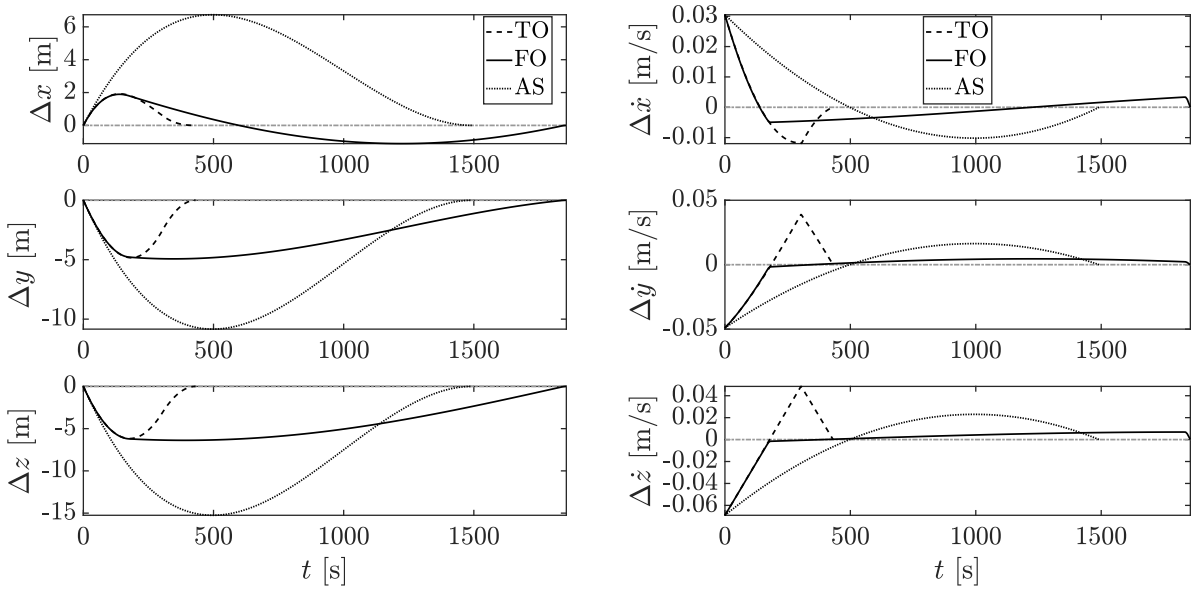

Fig. 10 Evolution of the position (left) and velocity (right) error with respect to the target manifold: comparison between the TO, FO and AS solutions.

The previous results are presented for the forward conversion, however they can be generalized to the backward control as well. In addition, an example application of a transfer with two impulsive maneuvers separated by a coasting arc is presented hereafter. The two ΔVs are selected in the same fashion as in the previous Monte Carlo simulation. Figure 12 shows the evolution of the error between the trajectory obtained via AS and the trajectory described by the transfer arc between the two impulsive maneuvers. The initial and final velocity errors match the initial and final impulsive maneuvers, allowing to retrieve exactly the desired initial and final states. The first part of the error trajectory

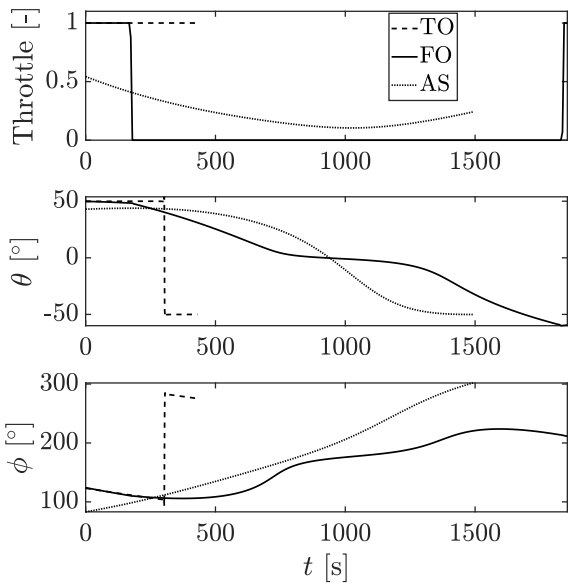

Fig. 11 Control history for a sample trajectory: comparison between the TO, FO and AS solutions.

is retrieved using the forward control laws to map the first impulsive maneuver. The required time to complete this conversion is obtained exploiting Eq. (37). After the maneuver is completed, a coasting arc can be observed, where no controls are executed and the trajectory follows natural unforced motion. The length of this coasting arc is selected randomly and can be reduced to zero. Finally, the third part of the trajectory exploits the backward controls. Also in this case the final time can be selected according to Eq. (37). The outcome of this simulation shows that it is possible to map any two-impulse transfer if the transfer time of the ideal impulsive approach is greater or equal to $2t_f$.

VI. Conclusions

This work presented an analytic control law to map an impulsive maneuver into a continuous thrust profile that achieves the same final trajectory in terms of positions and velocities to a good accuracy in case the nonlinearities of the problem are not dominant (i.e. circular target orbit, small relative distances), which is typical for close proximity operations. It also showed the possibility to map a two-impulse transfer exploiting the same control approach. In doing so, an analytic conservative bound for the thrust was also retrieved, which grants control laws that comply with the maximum thrust constraint. The selected third order polynomial shape functions for the controls may be a suboptimal selection, however they allow to achieve the desired outcome. Additional investigation of possible shape functions may yield better performance and constitute an interesting starting point for further research on the topic. In addition, the analytic solution was applied and compared against minimum time and minimum fuel controls. Due to its nature, the analytic control law outperforms the iterative optimal control solutions in terms of computational effort and memory required. Moreover, the lack of any iterative process makes it free of convergence issues, which is a desirable feature for

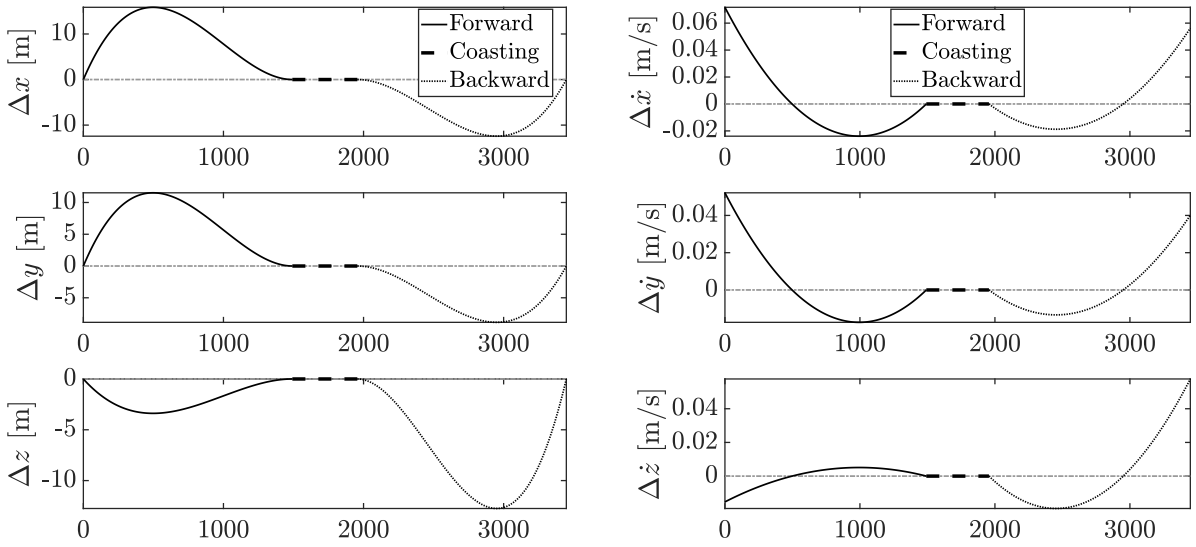

Fig. 12 Evolution of the position (left) and velocity (right) error obtained via the AS control conversion of a two-impulse transfer.

on-line implementation. To conclude, the analytic control law provided also a feasible good initial guess for all the iterative optimization algorithms, which eased convergence in all simulations.

References

[1] European Space Agency, *About Space Debris*, 2018 (accessed August 1, 2019). URL http://m.esa.int/Our_Activities/Space_Safety/Space_Debris/About_space_debris.

[2] Clohessy, W. H., and Wiltshire, R. S., "Terminal Guidance System for Satellite Rendezvous," *Journal of the Aerospace Sciences*, Vol. 27, 1960, pp. 653–658. https://doi.org/10.2514/8.8704.

[3] Woffinden, D., "On-orbit satellite inspection : navigation and delta-v analysis," Master's thesis, Massachussetts Institute of Technology, Department of Aeronautics and Astronautics, Cambridge, MA, 2005. URL https://dspace.mit.edu/handle/1721.1/28862.

[4] Williams, T., "Orbital Inspection Vehicle Trajectories Based on Line-of-Sight Maneuvers," *Acta Astronautica*, Vol. 50, 2002, pp. 49–53. https://doi.org/10.1016/S0094-5765(01)00140-0.

[5] Frey, G. R., Petersen, C. D., Leve, F. A., Kolmanovsky, I. V., and Girard, A. R., "Constrained spacecraft relative motion planning exploiting periodic natural motion trajectories and invariance," *Journal of Guidance, Control, and Dynamics*, Vol. 40, No. 12, 2017, pp. 3100–3115. https://doi.org/10.2514/1.G002914.

[6] Latombe, J. C., *Robot motion planning*, Springer US, Boston, MA, 1991, Chap. 1, pp. 1–57. https://doi.org/10.1007/978-1-4615-4022-9_1.

[7] Kavraki, L. E., Svestka, P., Latombe, J., and Overmars, M. H., "Probabilistic roadmaps for path planning in high-dimensional configuration spaces," *IEEE Transactions on Robotics and Automation*, Vol. 12, No. 4, 1996, pp. 566–580. https://doi.org/10.1109/70.508439.

[8] Starek, J. A., Açıkmeşe, B., Nesnas, I. A., and Pavone, M., *Spacecraft Autonomy Challenges for Next-Generation Space Missions*, Springer Berlin Heidelberg, Berlin, Heidelberg, 2016, pp. 1–48. https://doi.org/10.1007/978-3-662-47694-9_1.

[9] Starek, J. A., Schmerling, E., Maher, G. D., Barbee, B. W., and Pavone, M., "Real-time, propellant-optimized spacecraft motion planning under Clohessy-Wiltshire-Hill dynamics," *2016 IEEE Aerospace Conference*, IEEE Publisher, Piscataway, NJ, 2016, pp. 1–16. https://doi.org/10.1109/AERO.2016.7500704.

[10] Starek, J. A., Barbee, B. W., and Pavone, M., "A sampling based approach to spacecraft autonomous maneuvering with safety specifications," *Advances in the Astronautical Sciences*, Vol. 154, 2015, pp. 725–738.

[11] Francis, G., Collins, E., Chuy, O., and Sharma, A., "Sampling-Based Trajectory Generation for Autonomous Spacecraft Rendezvous and Docking," *AIAA Guidance, Navigation, and Control (GNC) Conference*, 2013. https://doi.org/10.2514/6.2013-4549.

[12] Surovik, D. A., and Scheeres, D. J., "Autonomous maneuver planning at small bodies via mission objective reachability analysis," *AIAA/AAS Astrodynamics Specialist Conference*, 2014, p. 4147. https://doi.org/10.2514/6.2014-4147.

[13] Capolupo, F., and Labourdette, P., "Receding-Horizon Trajectory Planning Algorithm for Passively Safe On-Orbit Inspection Missions," *Journal of Guidance, Control and Dynamics*, Vol. 42, No. 5, 2019, pp. 1023–1032. https://doi.org/10.2514/1.G003736.

[14] Capolupo, F., and Mast, S., "Sampling Based Receding Horizon Guidance for the Safe Inspection of a Tumbling Spacecraft," *Advances in the Astronautical Sciences*, Vol. 164, 2018, pp. 1149–1161.

[15] Tweedle, B., "Computer vision-based localization and mapping of an unknown, uncooperative and spinning target for spacecraft proximity operations," Ph.D. thesis, Massachussetts Institute of Technology, Department of Aeronautics and Astronautics, Cambridge, MA, 2013. URL https://dspace.mit.edu/handle/1721.1/85693.

[16] Pines, S., "Constants of the motion for optimum thrust trajectories in a central force field," *AIAA Journal*, Vol. 2, No. 11, 1964, pp. 2010–2014. https://doi.org/10.2514/3.2717.

[17] Handelsman, M., "Optimal free-space fixed-thrust trajectories using impulsive trajectories as starting iteratives." *AIAA Journal*, Vol. 4, No. 6, 1966, pp. 1077–1082. https://doi.org/10.2514/3.3607.

[18] Hazelrigg, G. A., and Lion, P. M., "Analytical determination of the adjoint vector for optimum space trajectories," *Journal of Spacecraft and Rockets*, Vol. 7, No. 10, 1970, pp. 1200–1207. https://doi.org/10.2514/3.30135.

[19] Kornhauser, A. L., Lion, P. M., and Hazelrigg, G. A., "An analytic solution for constant-thrust, optimal-coast, minimum-propellant space trajectories," *AIAA Journal*, Vol. 9, No. 7, 1971, pp. 1234–1239. https://doi.org/10.2514/3.6347.

[20] Fogel, J. A., Widner, M., Williams, J., and Batcha, A., "Multi-Impulse to Time Optimal Finite Burn Trajectory Conversion," *AIAA Scitech 2020 Forum*, 2020. https://doi.org/10.2514/6.2020-1691.

[21] Jesick, M., and Ocampo, C., "Automated Design of Optimal Finite Thrust Orbit Insertion with Ballistic Flyby Constraints," *Journal of Spacecraft and Rockets*, Vol. 51, No. 6, 2014, pp. 1872–1884. https://doi.org/10.2514/1.A32886.

[22] Di Lizia, P., Armellin, R., Bernelli-Zazzera, F., and Berz, M., "High order optimal control of space trajectories with uncertain boundary conditions," *Acta Astronautica*, Vol. 93, 2014, pp. 217 – 229. https://doi.org/10.1016/j.actaastro.2013.07.007.

[23] Topputo, F., and Bernelli-Zazzera, F., "Approximate Solutions to Nonlinear Optimal Control Problems in Astrodynamics," *ISRN Aerospace Engineering*, Vol. 2013, 2013. https://doi.org/10.1155/2013/950912.

[24] Bacon, R. H., "Logarithmic Spiral: An Ideal Trajectory for the Interplanetary Vehicle with Engines of Low Sustained Thrust," *American Journal of Physics*, Vol. 27, No. 3, 1959, pp. 164–165. https://doi.org/10.1119/1.1934788.

[25] Petropoulos, A. E., and Longuski, J. M., "Shape-Based Algorithm for the Automated Design of Low-Thrust, Gravity Assist Trajectories," *Journal of Spacecraft and Rockets*, Vol. 41, No. 5, 2004, pp. 787–796. https://doi.org/10.2514/1.13095.

[26] Wall, B. J., and Conway, B. A., "Shape-Based Approach to Low-Thrust Rendezvous Trajectory Design," *Journal of Guidance, Control, and Dynamics*, Vol. 32, No. 1, 2009, pp. 95–101. https://doi.org/10.2514/1.36848.

[27] Wall, B., Pols, B., and Lanktree, B., "Shape-based approximation method for lowthrust interception and rendezvous trajectory design," *Advances in the Astronautical Sciences*, Vol. 136, 2010, pp. 1447–1458.

[28] Taheri, E., and Abdelkhalik, O., "Fast Initial Trajectory Design for Low-Thrust Restricted-Three-Body Problems," *Journal of Guidance, Control, and Dynamics*, Vol. 38, No. 11, 2015, pp. 2146–2160. https://doi.org/10.2514/1.G000878.

[29] Fan, Z., Huo, M., Qi, J., and Qi, N., "Fast initial design of low-thrust multiple gravity-assist three-dimensional trajectories based on the Bezier shape-based method," *Acta Astronautica*, Vol. 178, 2021, pp. 233 – 240. https://doi.org/10.1016/j.actaastro.2020.09.020.

[30] De Pascale, P., and Vasile, M., "Preliminary Design of Low-Thrust Multiple Gravity-Assist Trajectories," *Journal of Spacecraft and Rockets*, Vol. 43, No. 5, 2006, pp. 1065–1076. https://doi.org/10.2514/1.19646.

[31] Novak, D. M., and Vasile, M., "Improved Shaping Approach to the Preliminary Design of Low-Thrust Trajectories," *Journal of Guidance, Control, and Dynamics*, Vol. 34, No. 1, 2011, pp. 128–147. https://doi.org/10.2514/1.50434.

[32] Xie, C., Zhang, G., and Zhang, Y., "Shaping Approximation for Low-Thrust Trajectories with Large Out-of-Plane Motion," *Journal of Guidance, Control, and Dynamics*, Vol. 39, No. 12, 2016, pp. 2780–2789. https://doi.org/10.2514/1.G001795.

[33] Schaub, H., and Junkins, J. L., *Analytical Mechanics of Space Systems*, 2nd ed., AIAA Education Series, Reston, VA, 2009, Chap. 14, pp. 676–681. https://doi.org/10.2514/4.867231.

[34] Topputo, F., and Zhang, C., "Survey of Direct Transcription for Low-Thrust Space Trajectory Optimization with Applications," *Abstract and Applied Analysis*, Vol. 2014, 2014, p. 15. https://doi.org/10.1155/2014/851720.

[35] Betts, J. T., "Survey of Numerical Methods for Trajectory Optimization," *Journal of Guidance, Control, and Dynamics*, Vol. 21, No. 2, 1998, pp. 193–207. https://doi.org/10.2514/2.4231.